

Dense, Fe-rich Ejecta in Supernova Remnants DEM L238 and DEM L249: A New Class of Type Ia Supernova?

Kazimierz J. Borkowski

Department of Physics, North Carolina State University, Raleigh, NC 27695

kborkow@ncsu.edu

Sean P. Hendrick

Department of Physics, Millersville University, Millersville, PA 17551

Stephen P. Reynolds

Department of Physics, North Carolina State University, Raleigh, NC 27695

ABSTRACT

We present observations of two LMC supernova remnants (SNRs), DEM L238 and DEM L249, with the *Chandra* and *XMM-Newton* X-ray satellites. Bright central emission, surrounded by a faint shell, is present in both remnants. The central emission has an entirely thermal spectrum dominated by strong Fe L-shell lines, with the deduced Fe abundance in excess of solar and not consistent with the LMC abundance. This Fe overabundance leads to the conclusion that DEM L238 and DEM L249 are remnants of thermonuclear (Type Ia) explosions. The shell emission originates in gas swept up and heated by the blast wave. A standard Sedov analysis implies about $50 M_{\odot}$ in both swept-up shells, SNR ages between 10,000 and 15,000 yr, low ($\lesssim 0.05 \text{ cm}^{-3}$) preshock densities, and subluminal explosions with energies of 3×10^{50} ergs. The central Fe-rich supernova ejecta are close to collisional ionization equilibrium. Their presence is unexpected, because standard Type Ia SNR models predict faint ejecta emission with short ionization ages. Both SNRs belong to a previously unrecognized class of Type Ia SNRs characterized by bright interior emission. Denser than expected ejecta and/or a dense circumstellar medium around the progenitors are required to explain the presence of Fe-rich ejecta in these SNRs. Substantial amounts of circumstellar gas are more likely to be present in explosions of more massive Type Ia progenitors. DEM L238, DEM L249, and similar SNRs could be remnants of “prompt” Type Ia explosions with young (~ 100 Myr old) progenitors.

Subject headings: ISM: individual (B0534-70.5, B0536-70.6) — supernova remnants — X-rays: ISM — supernovae: general

1. Introduction

Heavy elements are produced in stars and then injected into the interstellar medium (ISM) by the combined action of stellar winds and stellar explosions. Thermonuclear and core-collapse explosions are dominant sources of heavy elements, and they govern the evolution of chemical abundances in galaxies. Thermonuclear (Type Ia) explosions inject iron-rich supernova (SN) ejecta into the ISM, while ejecta of core-collapse (CC) SNe contain large quantities of oxygen and other α -elements. Heavy elements are dispersed by remnants of SNe and eventually mix with the ambient ISM, forming subsequent generations of stars. The O/Fe (or more generally α -elements/Fe) ratio depends on the relative frequency of CC and Type Ia explosions, and on how a galaxy has evolved in the past. It is now well established that this ratio varies among galaxies. In particular, the α /Fe ratio is lower in the Magellanic Clouds (MCs) than in our Galaxy (e.g., Pompéia et al. 2006). This suggests that chemical enrichment by Type Ia SNe has been relatively more important in the MCs than in our Galaxy. It is not clear whether this is caused by an increased frequency of Type Ia versus CC explosions in the MCs (Tsujimoto et al. 1995) or by differences in evolutionary histories between the MCs and our Galaxy (Pagel & Tautvaišienė 1998). Our poor understanding of progenitors of Type Ia explosions is a significant problem as well; the recent proposal of a new class of “prompt” Type Ia SNe (Mannucci et al. 2006; Sullivan et al. 2006) associated with relatively young (~ 100 Myr) stars may force reevaluation of current ideas about the poorly understood chemical evolution of the MCs.

Studies of remnants of Type Ia explosions in the MCs allow us to observe injection of Fe into the ISM directly and to study SN ejecta in detail, leading to a better understanding of Type Ia explosions and the enrichment of the MCs in heavy elements. Tuohy et al. (1982) discovered four supernova remnants (SNRs) in the Large Magellanic Cloud (LMC) with strong Balmer lines of hydrogen and weak forbidden lines of heavy elements; such Balmer-dominated remnants are believed to be of Type Ia origin. X-ray observations with the *Advanced Satellite for Cosmology and Astrophysics (ASCA)* confirmed a Type Ia origin for Balmer-dominated SNRs 0509-67.5 and 0519-69.0 by detecting strong Fe lines in their X-ray spectra (Hughes et al. 1995). Their ages are 400 and 600 yr, respectively, based on the recent discovery of light echoes from these explosions (Rest et al. 2005). The other two Balmer-dominated SNRs, DEM L71 and 0548-70.4, were also found to be rich in Fe (Hughes et al. 2003; Hendrick et al. 2003). There are several other Type Ia SNRs in the MCs, as indicated by their Fe overabundance. The bright SNR N103B is only ~ 1000 yr old, based on one detected light echo (Rest et al. 2005); its origin is still under debate, with van der Heyden et al. (2002) and Lewis et al. (2003) advocating a CC and Type Ia origin, respectively.

Most progenitors of Type Ia SNe are believed to belong to old stellar populations.

Because at most a modest amount of circumstellar material may be associated with the pre-explosion evolution of their low-mass progenitors, SN ejecta dissipate their kinetic energy mostly interacting with the ambient ISM. Lack of a dense circumstellar medium for most Type Ia SNe is consistent with the absence of radio emission from SNe Ia (Weiler et al. 2002). Type Ia SN progenitors are usually located far from clumpy star formation regions and generally explode in a relatively uniform diffuse ISM. Remnants of historical Type Ia SNe of Tycho and 1006 indeed exhibit rather smooth outer blast waves. Badenes et al. (2006) successfully modeled the Tycho X-ray spectrum with SN ejecta colliding with an ambient medium of constant density, finding good agreement for delayed-detonation models of Type Ia explosions. This encouraging agreement gives credence to the conventional wisdom in which most Type Ia SNRs arise from the interaction of SN ejecta with a rather uniform ambient medium, without needing to invoke the presence of dense circumstellar material in the immediate vicinity of their progenitors. Hydrodynamic models for such an interaction have been considered in the past (e.g., Dwarkadas & Chevalier 1998), and an extensive grid of models (including synthetic X-ray spectra) has become recently available (Badenes et al. 2003, 2005, 2006).

We present *Chandra* and *XMM-Newton* observations of two moderately ($\sim 10^4$ yr) old SNRs in the LMC, DEM L238 (B0534-70.5) and DEM L249 (B0536-70.6), which unexpectedly reveal the presence of Fe in their interiors, presumably produced by thermonuclear explosions of their progenitors. These 3'-diameter SNRs have been previously studied at optical and X-ray wavelengths (Mathewson et al. 1983; Williams et al. 1999), but these studies have not revealed anything unusual, except for the X-ray emission enhancement in their interiors. We find that the presence of Fe-rich ejecta at their centers is not consistent with the standard Type Ia SNR models just mentioned. The presence of denser than expected material in the vicinity of their SN progenitors or in SN ejecta is required. We discuss several possible scenarios that could explain this finding.

2. Observations and Imaging

X-ray observations with *XMM-Newton* were done on 2003 July 23, with the primary target DEM L238 located at the center of the European Photon Imaging Camera (EPIC) MOS and pn cameras. The total exposure time was 43.5 ks, and the Medium filter was used. We used the *XMM-Newton* Science Analysis System (SAS) software, version 6.5.0 to screen data for periods of high flare events, extracted images and spectra, and generated primary and secondary spectral response files. After screening of the data for flares, the effective exposure time was 17.4 ks for the pn camera, and 21.8 ks each for the MOS1 and

MOS2 cameras. We combined EPIC MOS and pn events to create an X-ray image (Fig. 1), not corrected for variations in the effective exposure time across the EPIC field of view. Linear features seen in this image are artifacts at boundaries between individual CCD chips comprising pn and MOS cameras.

In addition to our primary target DEM L238, SNR DEM L249 is also located in the EPIC field of view (Fig. 1). Both SNRs exhibit shells of soft X-ray emission surrounding central emission enhancements with harder X-ray spectra. (The shell morphologies seen in Fig. 1 have been slightly distorted by linear artifacts located at CCD boundaries crossing both shells.) Patchy emission seen in optical images (Mathewson et al. 1983) coincides with the soft X-ray-emitting shells; this is the swept-up ISM. Optical emission presumably traces localized dense regions where the blast wave slowed down and became radiative; the soft X-ray-emitting shell reveals the bulk of the swept-up ISM gas heated to X-ray-emitting temperatures by the primary blast wave.

Chandra observed DEM L238 for 59.2 ks on 2003 October 25–26, with the ACIS S3 chip. DEM L249 was in the field of view of the ACIS I2 and I3 chips, so high spatial resolution images are available for both SNRs. We used the *Chandra* X-ray analysis software CIAO, version 3.3 to screen data for periods of high background, extracted images and spectra, and generated spectral response files. Very faint mode was used to reduce the particle background. After screening, the effective exposure time was 50.4 ks for DEM L238 and 47.5 ks for DEM L249. *Chandra* images of DEM L238 and DEM L249 are shown in Figures 2 and 3. No correction has been applied to account for variations of the effective exposure time across the ACIS chips.

The high spatial resolution *Chandra* image of DEM L238 shows the separation between the soft X-ray-emitting shell and the harder interior emission more clearly. The interior emission is elliptical in shape, offset from the center of the shell toward the southwest. The shell and the central emission partially overlap. The soft X-ray-emitting shell of DEM L249 is faint, so only its brightest sections are seen in the *Chandra* image. The boundary between the I2 and I3 chips runs diagonally (southeast-northwest) up across the image, between the northeast shell and the central emission; this produces a linear artifact in the remnant's X-ray image.

A montage of high-quality narrowband optical images obtained in the Magellanic Cloud Emission Line Survey¹ (MCELS; Smith et al. 2000) is shown for each SNR in Figures 2 and 3. Optical emission and soft X-rays in DEM L238 have similar shell-like morphologies with

¹Preliminary data sets and description of this survey can be found online at <http://www.ctio.noao.edu/mcels>.

significant departures from a spherical shape, but they do not correlate well at small spatial scales. This is expected as optical emission is produced in slow radiative shocks and traces the location of dense ISM, while X-rays are emitted by gas heated to high temperatures in much faster nonradiative shocks. No optical emission is associated with the interior X-ray emission in DEM L238 (Fig. 2). DEM L249 is much more asymmetric in the optical, elongated in the southwest-northeast direction. Optical filaments are present at its center, but there is only a weak correlation between them and the central X-ray emission. The soft X-ray-emitting gas in the northeast and southwest (Figs. 1 and 3) again matches well with the optically emitting gas on large spatial scales, but poorly on small scales. Somewhat faster radiative shocks in the northwest than in the southeast are implied by the predominance of [O III] λ 5007 emission in the northwest, and its weakness relative to [S II] $\lambda\lambda$ 6716, 6731 and H α emission in the southeast. A large-scale northwest-southeast density gradient in the ISM is likely responsible for these differences in the radiative shock speeds. Soft X-ray emission farther northwest, seen only in more sensitive *XMM-Newton* observations (Fig. 1), has no visible optical counterpart, presumably because the ISM density there is too low for the formation of radiative shocks.

3. Spectral analysis

We extracted central and shell spectra from *XMM-Newton* and *Chandra* data in order to deduce the properties of the blast waves and establish the nature of the interior emission in DEM L238 and DEM L249. The central extraction regions are shown in Figures 1 and 2. The *Chandra* shell region of DEM L238 encompasses the whole remnant minus its central region. Background spectra were extracted from adjacent, point-source-free regions of the same CCD chips. Spectral analysis was performed with XSPEC, version 12 (Arnaud 1996). We used both the nonequilibrium ionization (NEI), version 2.0 thermal models, based on the astrophysical plasma emission code and database (APEC/APED; Smith et al. 2001) and augmented by addition of inner-shell processes (Badenes et al. 2006), and the collisional ionization equilibrium APEC models. Spectra were binned to a minimum 25 counts bin⁻¹ in order to allow the use of χ^2 statistics.

3.1. Shell Emission

The interior and shell *Chandra* spectra of DEM L238 have 6676 and 3772 counts in the energy range 0.4–3.0 keV, or 6120 and 2380 counts after background subtraction. They differ greatly (Fig. 4), as expected from the pronounced color differences seen in Figures 1 and

2. The presence of emission lines in these spectra shows that the observed X-ray emission is of thermal origin. We fit the shell spectrum with a standard Sedov model with 0.4 solar (cosmic) abundances appropriate for the LMC. We used a two-component absorption model: foreground Galactic absorption with the column density of $N_H = 6 \times 10^{20} \text{ cm}^{-2}$ appropriate for this location on the sky (Staveley-Smith et al. 2003), and the LMC absorption with 0.4 solar abundances that we allowed to vary. The best fit is shown in Figure 4, with postshock mean temperature $kT_s = 0.40 \text{ keV}$ [(0.34, 0.53), 90% confidence interval], postshock electron temperature $kT_e = 0.11(0.0, 0.34) \text{ keV}$, ionization age $\tau = n_e t_{SNR} = 9.4(7.1, 14) \times 10^{11} \text{ cm}^{-3} \text{ s}$ (where n_e is the postshock electron density and t_{SNR} is the SNR age), and emission measure $EM = \int n_e n_H dV$ of $4.4 \times 10^{57} \text{ cm}^{-3}$ (at the assumed 50 kpc distance to the LMC). The shock speed V_s corresponding to a temperature of 0.40 keV is 600 km s^{-1} . No internal absorption within the LMC was necessary. While the Sedov fit with standard LMC abundances was statistically acceptable, an inspection of Figure 4 reveals that the Sedov model underpredicts the observed spectrum at low energies, and the $K\alpha/\text{Ly}\alpha$ line ratio of O is underestimated. Apparently there is a substantial amount of low-temperature plasma in the blast wave of DEM L238, in excess of what is predicted by a standard Sedov model. This is likely caused by variations in the blast wave speed around the remnant’s periphery, with the very soft X-ray emission coming from shocks with speeds less than the average blast wave speed of 600 km s^{-1} , but more than $\sim 100 \text{ km s}^{-1}$ expected for radiative shocks seen in optical.

In the Sedov dynamical model, $V_s = 2R_s/5t_{SNR}$, where $R_s = 80''$ (20 pc at 50 kpc distance) is the remnant’s radius. With the current shock speed of 600 km s^{-1} , the estimated remnant’s age t_{SNR} is equal to 13,500 yr. The preshock density n_0 ahead of the blast wave in DEM L238 can be estimated from the Sedov EM (e.g., Hamilton et al. 1983). Our Sedov spectral fit to the shell spectrum of DEM L238 (Fig. 4) excluded the central region shown in Figure 2, so that we need to correct the EM obtained in this fit to account for the incomplete spatial coverage of the remnant. An X-ray-emitting shell in a Sedov model may be approximated as a geometrically thin shell, and the correction factor is equal to $1/(1 - 2f_c)$, where f_c is the fraction of the solid angle occupied by the central region as seen from the remnant’s center, and the factor of 2 accounts for the front and back sections of the shell (we assumed a spherically symmetric SNR). After 60% correction to the EM, we arrive at $n_0 = 0.05 \text{ cm}^{-3}$. The estimated swept-up mass is $60 M_\odot$. The inferred kinetic energy E_k of the explosion is equal to $3.3 \times 10^{50} \text{ ergs}$. This is less than the canonical explosion energy of 10^{51} ergs , but in agreement with energies derived for several Type Ia SNRs in the LMC (Hendrick et al. 2003; Ghavamian et al. 2003). The product of n_0 and t_{SNR} is equal to $2 \times 10^{10} \text{ cm}^{-3} \text{ s}$, about 40 times less than the Sedov ionization age derived directly from the spectral fit. This suggests longer t_{SNR} and/or higher n_0 than estimated above. Dense ISM is present near DEM L238, as evidenced by large-scale radiative shocks seen in the optical

(Fig. 2), and the X-ray emission might be produced by gas with densities higher than 2 cm^{-3} (this requires a lower volume filling factor than the 1/4 appropriate for the standard Sedov model). These inconsistencies of the Sedov model cast some doubt on its validity for DEM L238. A crucial assumption in this model is the uniformity of the ambient medium around the SN progenitor; this assumption might be appropriate for most Type Ia explosions but would be incorrect for a massive progenitor of a CC SN. A CC progenitor is expected to modify the ambient medium through the action of its stellar winds prior to the SN explosion. In this case, inferences based on the Sedov analysis could be incorrect.

The X-ray-emitting shell in DEM L249 is too faint for spectral analysis with *Chandra*, so we used *XMM-Newton* data for this purpose. In Figure 5 we contrast *XMM-Newton* EPIC pn spectra of the shell and the interior emission. The spatially integrated *Chandra* spectrum is also shown. This *Chandra* spectrum does not completely include the faint shell sections in the northeast and northwest, and it is dominated by the bright interior emission. The difference between the central and shell spectra is again obvious. We extracted the shell spectra from the northeast and south part of the shell, not from the fainter northwest section seen in Figure 1, where the SNR is not apparent on the MCELS optical images (Fig. 3) and where the blast speed might be higher than in the northeast and south. The total numbers of counts in the 0.4–3.0 keV range were 815, 321, and 309 for pn, MOS1, and MOS2 detectors, respectively. After background subtraction, these numbers were reduced to about 600 counts for pn, and ~ 225 each for MOS detectors. Because of the low numbers of counts, we made joint fits to pn, MOS1, and MOS2 spectra with the Sedov model (only pn spectra are shown in Fig. 5). Foreground Galactic absorption with $N_H = 6 \times 10^{20} \text{ cm}^{-2}$ was assumed, based on H I observations by Staveley-Smith et al. (2003). A Sedov model fit with 0.4 solar abundances was not acceptable, primarily because this model could not reproduce Fe emission lines at $\sim 0.8 \text{ keV}$ seen in the pn shell spectrum of Figure 5. A better fit resulted by allowing the Fe abundance to vary, with the Ni abundance tied to Fe, although the lack of internal consistency between pn, MOS1, and MOS2 spectra prevented a statistically acceptable fit. This fit is shown in Figure 5. Again, no internal absorption in the LMC was required. The derived postshock temperature is 0.36 keV, corresponding to 550 km s^{-1} , and the ionization timescale $\tau = 2.1 \times 10^{11} \text{ cm}^{-3} \text{ s}$. The Fe abundance is 1.5 solar, significantly in excess of the LMC Fe abundance. The inferred Fe overabundance in the swept-up ISM might not be real. DEM L249 has relatively bright central emission with strong Fe L-shell emission (see Fig. 5) and a much fainter shell, and its far off-axis location, where the *XMM-Newton* point-spread function is quite broad, increases the potential for contamination of the shell spectrum by the central emission. In view of the rather poor photon statistics, we have not attempted to deconvolve the central and shell spectra. The derived shock speed in DEM L249 is only slightly lower than in DEM L238, while the ionization age is shorter by a factor of 4. These

similarities, as well as similar central spectra (cf. Figs. 4 and 5), suggest these two SNRs are alike in many respects.

3.2. Central Emission

Central X-ray spectra of DEM L238 extracted from the *XMM-Newton* EPIC pn and combined MOS detectors and from the *Chandra* ACIS S3 chip are shown in Figure 6. (We present an average of MOS1 and MOS2 spectra for display purposes only; all fits were done using separate spectral responses for MOS1 and MOS2 detectors.) The pn, MOS, and ACIS S3 spectra differ in shape because of variations among individual CCD spectral responses. As can be seen in the high spatial resolution *Chandra* image of DEM L238 (Fig. 2, *left*), the soft X-ray-emitting shell and the harder interior emission overlap spatially. The central spectra are then comprised of a sum of the shell and interior emission, so in addition to a single `vpshock` model (Borkowski et al. 2001) we also used a two-component model in spectral fitting. For the shell component, we fixed parameter values to those found in the fits to the shell spectrum described above, allowing only the normalization of this component to vary. For the second interior component, we initially used various NEI models, but the long ionization timescales derived from two-component fits always suggested that gas at the center is close to collisional ionization equilibrium (CIE). We found that use of the CIE APEC thermal model produced as good statistical fits as NEI thermal models, so we present here fits with the APEC model (plus the Sedov shell component). We assumed the same interstellar absorption, $N_H = 6 \times 10^{20} \text{ cm}^{-2}$, as in fits to the shell spectrum. We made separate fits to *Chandra* ACIS S3, *XMM-Newton* EPIC pn spectra, and joint fits to *XMM-Newton* EPIC MOS1 and MOS2 spectra.

All fits with the APEC model with 0.4 solar abundances appropriate for the LMC failed to produce acceptable results. Large residuals seen near 0.9 keV suggest the presence of stronger than expected Fe L-shell lines. We obtained statistically acceptable fits by allowing the Fe abundance to vary, with the Ni abundance tied to Fe. These fits are presented in Table 1 and Figure 6. The Fe L-shell line complex at ~ 0.9 keV is prominent in all three spectra. The X-ray-emitting gas at the center of DEM L238 is rich in Fe. This appears to be a robust result, as we arrived at a similar Fe overabundance when we allowed for either underionized (`vpshock` and `vnei` NEI models in XSPEC) or overionized (custom-made XSPEC models) plasmas. The most straightforward interpretation of this result is that we are seeing Fe-rich SN ejecta, presumably produced in a thermonuclear (Type Ia) explosion.

The relative abundances of elements in SN ejecta are of great interest, but their de-

termination is difficult in DEM L238 because of the spatial overlap of the interior and the shell emission and uncertainties in atomic data for Fe L-shell lines. For the models shown in Figure 6 and listed in Table 1, the O/Fe ratio with respect to the solar value of Anders & Grevesse (1989), [O/Fe] is 0.29, 0.31, and 0.26 in fits to *XMM-Newton* MOS1+MOS2, pn, and *Chandra* spectra, respectively. This gives the O/Fe ratio of 5.3, 5.7, and 4.7 by number, higher than found in most Type Ia SN models (e.g., the O/Fe ratio ranges from 0.25 to 0.8 in models of Iwamoto et al. 1999), but far lower than the expected value of order 70 for CC events. However, we find that even very low O/Fe ratios are consistent with observations, based on additional fits (not shown) where we allowed the O abundance within ejecta to vary. In these fits no O was required; however, errors were large. In our two-component model fits, the shell component with the prominent O lines dominates at low energies, while the interior ejecta component is very strong in the Fe L-shell lines. The shell contribution is not accurately known, so determination of the O/Fe ratio within the ejecta is coupled to the problem of separation of the shell and ejecta contributions. This results in relatively large statistical errors on the derived O/Fe ratio.

A reliable determination of elemental abundances in the Fe-rich gas of DEM L238 is also made difficult by continuing uncertainties in atomic data for Fe L-shell lines. This problem is particularly severe for elements such as Ne and Mg, whose X-ray lines overlap with the Fe lines at the low spectral resolution of the CCD detectors. We made additional fits (not shown), in which we allowed Ne and Mg abundances to vary. In these fits, no Ne was required, while the Mg abundance was approximately solar. These two-component fits with variable Ne and Mg abundances were of much better quality than the two-component fits presented in Table 1, as judged by their lower χ^2 values. The low Ne abundance could be real, consistent with low Ne abundances in Type Ia SN models. The relatively high Mg abundance might be spurious, because a number of Fe lines spectrally overlapping with Mg lines are missing in APEC and other existing X-ray spectral codes (Brickhouse et al. 2000). Such deficiencies in Fe L-shell atomic data pose serious problems for studies of the ejecta composition in DEM L238.

It is also difficult to determine whether we observe pure heavy-element ejecta, or whether substantial mixing occurred with gas with normal LMC abundances, where most electrons are contributed by H and He. Mixing was implicitly assumed when we used the APEC model with abundances of elements other than Fe and Ni fixed to 0.4 solar in fits to the central emission. In this case, about $\sim 40f^{1/2} M_{\odot}$ (including $\sim 0.1f^{1/2} M_{\odot}$ of Fe) would be present in the central region (f denotes the unknown filling fraction of the X-ray-emitting gas). This mass estimate should be considered as an upper limit, because errors in the determination of the Fe abundance are large. In particular, we believe that the true upper limits on the Fe abundance are much larger than the statistical upper limits listed in Table 1. Our spectral

model for the Fe L-shell emission is incomplete, and we expect this incompleteness to become increasingly important with the increasing Fe abundance. The formal upper limits on the Fe abundance derived from the χ^2 analysis may then be highly misleading. We do not exclude the possibility that ejecta consist of pure Fe, in which case as much as $\sim 1 M_{\odot}$ of Fe could be present at the center of DEM L238. The most likely intermediate case involves several solar masses of gas, including a few tenths M_{\odot} of Fe.

Central X-ray spectra of DEM L249 extracted from the *XMM-Newton* EPIC pn and combined MOS detectors and the spatially integrated *Chandra* spectrum are shown in Figure 7. There are 2290 (2130), 1526 (1400), and 3171 (2180) counts in these spectra before (after) the background subtraction. We used the same techniques in analyzing these spectra as for DEM L238. Results of spectral fits are presented in Table 2 and Figure 7. These spectra are dominated by Fe L-shell emission, and again enhanced Fe abundances are required. Determination of reliable O, Ne, and Mg abundances with respect to Fe within the ejecta faces the same obstacles as in DEM L238, and the derived abundance ratios are the same as in DEM L238 (albeit within large errors). The gas temperature is slightly lower than in DEM L238, producing a noticeable shift in the centroid of the Fe L-shell emission toward lower energies when compared with DEM L238. DEM L249 appears to be very similar to DEM L238, but at a slightly more advanced evolutionary stage, as indicated by its larger angular size, slower shock speed, cooler Fe-rich gas at its center, and lower X-ray flux.

4. Discussion

Our main finding is the discovery of Fe-rich gas in the centers of the moderately old ($\sim 10^4$ yr) SNRs DEM L238 and DEM L249. An important property of this gas is its very long ionization age; we found the interior X-ray spectra of both SNRs well fit by collisional equilibrium ionization models. Such remnants, with central Fe overabundances and long ionization timescales, have been found before. In addition to four Balmer-dominated SNRs and N103B mentioned in § 1, several other Fe-rich remnants have been discovered in the MCs: 0534-69.9 (Hendrick et al. 2003); DEM S128, IKT5, and IKT25 (van der Heyden et al. 2004); DEM L316A (Nishiuchi et al. 2001; Williams & Chu 2005); and 0454-67.2 (Seward et al. 2006). Among them, DEM L316A is most similar to DEM L238 and DEM L249, as the Fe-rich gas at its center is in ionization equilibrium, and a swept-up shell is present. The SMC SNRs DEM S128 and IKT 5 also have Fe-rich gas in CIE, but their shells have not been detected by *XMM-Newton*. There is then a whole class of remnants with centrally located Fe-rich gas in CIE, and faint or undetectable X-ray shells, making up a substantial fraction of all MC Type Ia SNRs.

It is usually assumed that the presence of Fe-rich ejecta is a signature of a Type Ia explosion. However, DEM L238 and DEM L249 exhibit a number of puzzling properties that are hard to understand in the framework of the standard Type Ia models mentioned in § 1. The long ionization times of the Fe-rich gas imply that the gas density has had to be high enough in the past. In the standard Type Ia models of Badenes et al. (2003, 2005, 2006), this can be accomplished only by increasing the ambient medium density (assumed to be constant). But the predicted shell emission in such models is orders of magnitude brighter than observed. If we use instead the blast wave properties derived from the Sedov fits to the shell emission, which imply low ISM densities, then the Fe-rich ejecta are always at low densities and ionization timescales are short. We demonstrate this by considering simple models with an exponential density profile and uniform ambient ISM (Dwarkadas & Chevalier 1998), with ejecta mass of $1.4 M_{\odot}$ composed of pure Fe, and with $E_k = 3.3 \times 10^{50}$ ergs, $n_0 = 0.05 \text{ cm}^{-3}$, and $t_{SNR} = 13,500 \text{ yr}$ derived from the Sedov analysis of DEM L238. We performed our one-dimensional simulations with the Virginia Hydrodynamics PPM (VH-1) code. This code was written and tested by the Virginia Numerical Astrophysics Group and is based on the Lagrangian-Remap version of the piecewise parabolic method developed by Colella & Woodward (1984). We employed a simplified method devised for multidimensional hydrodynamic simulations coupled with NEI calculations to follow Fe ionization states within the ejecta. We used the NEI, version 1.1 spectral code in XSPEC to calculate X-ray spectra (Fe L-shell atomic data in all NEI models in XSPEC are based on theoretical calculations of Liedahl et al. 1995). (The low-ionization timescales we found led us to use NEI, version 1.1 instead of the APEC-based version 2.0, because the former includes more of the lower ionization transitions.) The calculated X-ray spectra are compared with the central *Chandra* X-ray spectrum of DEM L238 in Figure 8. The failure of a standard Type Ia model is obvious, as the shocked Fe in the model is underionized and the ejecta X-ray emission is more than an order of magnitude too faint. An inspection of more realistic Type Ia models of Badenes et al. (2003, 2005, 2006) confirms this conclusion. The fundamental problem is that the density of the Fe-rich ejecta is too low.

The presence of denser than expected gas at the center of DEM L238 and DEM L249 might be explained if they resulted instead from CC explosions. Dense circumstellar medium (CSM) has been found close to progenitors of CC explosions, including SN 1987A. The CSM will be shocked early in a SNR’s evolution, and at late times the shocked CSM gas will be near CIE conditions, or maybe even recombining (Itoh & Masai 1989). After the passage through the CSM, the blast wave will enter a bubble blown by the SN progenitor during its main-sequence stage, and then it will hit a dense swept-up ISM shell surrounding the tenuous bubble. This could explain the presence of dense, optically-emitting material in Figures 2 and 3. The problem with this hypothesis is that Fe is not the dominant nuclear burning

product of CC explosions. The observed Fe overabundance would require the operation of a selective mechanism that would enhance emission from Fe and suppress emission from abundant elements such as O. This is not likely, and we reject a CC origin for DEM L238 and DEM L249. Another possibility involves an increased Fe abundance in the LMC gas itself, but there is no evidence for such large Fe overabundances in the LMC.

Perhaps Fe is produced in thermonuclear explosions, but the ejecta structure, the structure of the ambient medium, or both are quite different than in the standard Type Ia models (Dwarkadas & Chevalier 1998; Badenes et al. 2003, 2005, 2006). Type Ia progenitors are still poorly understood, and there is growing evidence for the existence of peculiar Type Ia SNe. A subluminous class of Type Ia SNe was recently discovered (Jha et al. 2006), exemplified by SN 2002cx, with low expansion velocities and the presence of relatively dense partially burned or unburned material at their centers. Dense, slow-moving Fe-rich gas is likely to be prominent in the interiors of remnants of such explosions, although detailed comparisons with observations of DEM L238 and DEM L249 must await a better understanding of this peculiar class of SNe. All five known members of the class of SN 2002cx exploded in blue, star-forming spiral galaxies, making them candidates for the prompt explosions suggested by Mannucci et al. (2006) and Sullivan et al. (2006). This and perhaps other classes of prompt Type Ia SNe must originate from more massive progenitors than standard, much older Type Ia SNe. Such progenitors are more likely to be surrounded by circumstellar material formed by ejection of the massive progenitor envelope prior to the explosion. Several Type Ia SNe have been found to be surrounded by dense CSM, including SN 2002ic (Hamuy et al. 2003), although such SNe are infrequent. Among remnants of historical supernovae, Kepler’s SNR shows evidence for dense circumstellar material (e.g., Blair 2005), and Kinugasa & Tsunemi (1999) suggested a Type Ia origin for this remnant based on a high Fe abundance derived from its *ASCA* X-ray spectrum. Finally, if the companion to a white dwarf was a massive asymptotic giant branch star at the time of the white dwarf explosion, its entire envelope could have been stripped by SN ejecta (Marietta et al. 2000). At late stages of SNR evolution, an Fe-contaminated envelope is expected to appear as dense Fe-rich gas close to the center of the SNR. An asymmetric morphology is expected in this case.

Chu & Kennicutt (1988) associated DEM L238 and DEM L249 with old (Population II) stars and Type Ia explosions, because a CC origin for these SNRs is unlikely based on their large projected distances from OB associations in the LMC. But $\sim 10^8$ yr old Type Ia progenitors belonging to the young stellar population would be too old to be associated with the much younger ($\lesssim 10^7$ yr) massive stars in OB associations. Cepheid variables are better tracers of stars with such ages, and their spatial distribution is not correlated with OB associations and is only very marginally correlated with older star clusters (Battinelli & Efremov 1999). DEM L238 and DEM L249 are located in the LMC bar with a high Cepheid

density (Alcock et al. 1999). It is possible that their progenitors were born in the same star formation episode as Cepheids, although older progenitors belonging to Population I (or even to Population II) cannot be excluded, as this region of the LMC consists of a mixture of stellar populations.

DEM L238 and DEM L249 might belong to the same SNR population as young Fe-rich SNRs N103B and Kepler. The circumstellar gas in optically emitting N-rich radiative shocks in Kepler is dense; Blair et al. (1991) estimated preshock densities in the $100 - 1000 \text{ cm}^{-3}$ range. This gas traces the densest parts of the clumpy circumstellar material, where radiative cooling is important. The primary non-radiative blast wave propagates through the bulk of the strongly asymmetric CSM, with preshock densities as high as $\sim 10 \text{ cm}^{-3}$ (Blair et al. 1991). Optically emitting radiative shocks with high (180 cm^{-3}) preshock densities are also present in N103B (Russell & Dopita 1990). Unlike in Kepler, the N abundance is similar to its ISM value, but densities are much higher than in the surrounding H II region N103 or in the general diffuse ISM. Such high densities are more typical of molecular clouds, but there are no known nearby molecular clouds associated with N103B (Fukui et al. 1999; Mizuno et al. 2001). These high densities and the high X-ray luminosity of N103B suggest the presence of dense circumstellar gas, although an ISM origin for the ambient gas cannot be ruled out at this time. N103B may be associated with the nearby double star cluster NGC 1850. The main cluster is 50 Myr old, but the second cluster is very young (2–5 Myr; Caloi & Cassatella 1998). Optical observations revealed an enhancement in the N103B H α emission at the radial velocity of the H II region N103 produced by young stars in NGC 1850 and its surroundings (Chu & Kennicutt 1988). Chu & Kennicutt (1988) interpreted this as evidence for a blast wave interaction with ambient ISM gas, but an alternative explanation involves the CSM around a moderately old (50 Myr) SN progenitor with a radial velocity comparable to its parent cluster (and hence the H II region N103). Just like Kepler, N103B is strongly asymmetric at all wavelengths, with a compact and bright western hemisphere and a large and much fainter eastern hemisphere. The asymmetry in the ambient CSM has been invoked to explain the asymmetry of the Kepler SNR, and a similar explanation is likely for N103B. At an age of $\sim 10^4$ yr, both Kepler and N103B could still retain an imprint of the dense ambient CSM, and resemble DEM L238 and DEM L249.

In summary, *Chandra* and *XMM-Newton* observations revealed Fe-rich gas at the centers of LMC SNRs DEM L238 and DEM L249. While the Fe overabundance suggests Type Ia progenitors, the standard Type Ia models cannot explain the presence of relatively dense SN ejecta with long ionization timescales. At this time we do not understand the origin of these ejecta; one possibility involves prompt Type Ia explosions with progenitors more massive than average. The remnant of Kepler’s SN and the young LMC SNR N103B may belong to this category of Type Ia SNRs. Studies of remnants of such explosions in the MCs promise

to shed light on the nature of their poorly understood progenitors. The presence of such unusual progenitors may also force a reevaluation of the current chemical evolution models of the MCs, in view of the prominent role of Type Ia explosions in their evolution.

We thank John Blondin for his VH-1 hydrocode, and Paul Plucinsky for his help with planning *Chandra* observations. Optical images are courtesy of Sean Points, Chris Smith, and the Magellanic Cloud Emission Line Survey (MCELS) collaboration. This work was supported by NASA through grants NAG5-13641, SAO G03-4097X, and SAO AR5-6007X.

REFERENCES

- Alcock, C., et al. 1999, *AJ*, 117, 920
- Anders, E., & Grevesse, N., 1989, *GeCoA*, 53, 197
- Arnaud, K. A. 1996, in *Astronomical Data Analysis and Systems V*, eds. G.Jacoby & J.Barnes, ASP Conf. Series, v.101, 17
- Badenes, C., Borkowski, K. J., & Bravo, E. 2005, *ApJ*, 624, 198
- Badenes, C., Borkowski, K. J., Hughes, J. P., Hwang, U., & Bravo, E. 2006, *ApJ*, 645, 1373
- Badenes, C., Bravo, E., Borkowski, K. J., & Dominguez, I. 2003, *ApJ*, 593, 358
- Battinelli, P., & Efremov, Y. N. 1999, *A&A*, 346, 778
- Blair, W. P. 2005, in *Supernovae as Cosmological Lighthouses*, Eds. M. Turatto, S. Benetti, L. Zampieri, and W. Shea (San Francisco, Astronomical Society of the Pacific), p. 414
- Blair, W. P., Long, K., & Vancura, O. 1991, *ApJ*, 366, 484
- Borkowski, K. J., Lyerly, W. J., & Reynolds, S. P. 2001, *ApJ*, 548, 820
- Brickhouse, N. S., Dupree, A. K., Edgar, R. J., Liedahl, D. A., Drake, S. A., White, N. E., & Singh, K. P. 2000, *ApJ*, 530, 387
- Caloi, V., & Cassatella, A. 1998, *A&A*, 330, 492
- Chu, Y.-H., & Kennicutt, R. C., Jr. 1988, *AJ*, 96, 1874
- Colella, P., & Woodward, P. R. 1984, *J. Comput. Phys.*, 54, 174

- Dwarkadas, V. V., & Chevalier, R. A. 1998, *ApJ*, 497, 807
- Fukui, Y., et al. 1999, *PASJ*, 51, 745
- Ghavamian, P., Rakowski, C. E., Hughes, J. P., & Williams, T. B. 2003, *ApJ*, 590, 833
- Hamilton, A. J. S., Sarazin, C. L., & Chevalier, R. A., 1983, *ApJS*, 51, 115
- Hamuy, M., et al. 2003, *Nature*, 424, 651
- Hendrick, S. P., Borkowski, K. J., & Reynolds, S. P. 2003, *ApJ*, 593, 370
- van der Heyden, K. J., Behar, E., Vink, J., Rasmussen, A. P., Kaastra, J. S., Bleeker, J. A. M., Kahn, S. M., & Mewe, R. 2002, *A&A*, 392, 955
- van der Heyden, K. J., Bleeker, J. A. M., & Kaastra, J. S., 2004, *A&A*, 421, 1031
- Hughes, J. P., et al. 1995, *ApJ*, 444, L81
- Hughes, J. P., Ghavamian, P., Rakowski, C. E., & Slane, P. O. 2003, *ApJ*, 582, L95
- Itoh, H., & Masai, K. 1989, *MNRAS*, 236, 885
- Iwamoto, K., et al. 1999, *ApJS*, 125, 439
- Jha, S., Branch, D., Chornock, R., Foley, R. J., Li, W., Swift, B. J., Casebeer, D., & Filippenko, A. V. 2006, *AJ*, 132, 189
- Kinugasa, K., & Tsunemi, H. 1999, *PASJ*, 51, 239
- Lewis, K. T., Burrows, D. N., Hughes, J. P., Slane, P. O., Garmire, G. P., & Nousek, J. A. 2003, *ApJ*, 582, 770
- Liedahl, D. A., Osterheld, A. L., & Goldstein, W. H. 1995, *ApJ*, 438, L115
- Mannucci, F., Della Valle, M., & Panagia, N. 2006, *MNRAS*, 370, 773
- Marietta, E., Burrows, A., & Fryxell, B. 2000, *ApJS*, 128, 615
- Mathewson, D. S., Ford, V. L., Dopita, M. A., Tuohy, I. R., Long, K. S., & Helfand, D. J. 1983, *ApJS*, 51, 345
- Mizuno, N., et al. 2001, *PASJ*, 53, 971
- Nishiuchi, M., Yokugawa, J., Koyama, K., & Hughes, J. P. 2001, *PASJ*, 53, 99

- Pagel, B. E. J., & Tautvaišienė, G. 1998, *MNRAS*, 299, 535
- Pompéia, L., Hill, V., Spite, M., Cole, A., Primas, F., Romaniello, M., Pasquini, L., Cioni, M.-R., & Smecker-Hane, T. 2006, *A&A*, in press
- Rest, A., et al. 2005, *Nature*, 438, 1132
- Russell, S. C., & Dopita, M. A. 1990, *ApJS*, 74, 93
- Seward, F. D., Williams, R. M., Chu, Y.-H., Dickel, J. R., Smith, R. C., & Points, S. D. 2006, *ApJ*, 640, 327
- Smith, R. C., Leiton, R., & Pizarro, S. 2000, in *Stars, Gas and Dust in Galaxies: Exploring the Links*, ASP Conf. Proc., Vol. 221, Eds. D. Alloin, K. Olsen, & G. Galaz (San Francisco: Astronomical Society of the Pacific), 83
- Smith, R. K., Brickhouse, N. S., Liedahl, D. A., & Raymond, J. C. 2001, *ApJ*, 556, L91
- Staveley-Smith, L., Kim, S., Calabretta, M. R., Haynes, R. F., & Kesteven, M. J. 2003, *MNRAS*, 339, 87
- Sullivan, M., et al. 2006, *ApJ*, 648, 868
- Tsujimoto, T., Nomoto, K., Yoshii, Y., Hashimoto, M., Yanagida, S., & Thielemann, F.-K. 1995, *MNRAS*, 277, 945
- Tuohy, I. R., Dopita, M. A., Mathewson, D. S., Long, K. S., & Helfand, D. J. 1982, *ApJ*, 261, 473
- Weiler, K. W., Panagia, N., Montes, M. J., & Sramek, R. A. 2002, *ARAA*, 40, 387
- Williams, R. M., & Chu, Y.-H. 2005, *ApJ*, 635, 1077
- Williams, R. M., Chu, Y.-H., Dickel, J. R., Petre, R., Smith, R. C., & Tavaréz, M. 1999, *ApJS*, 123, 467

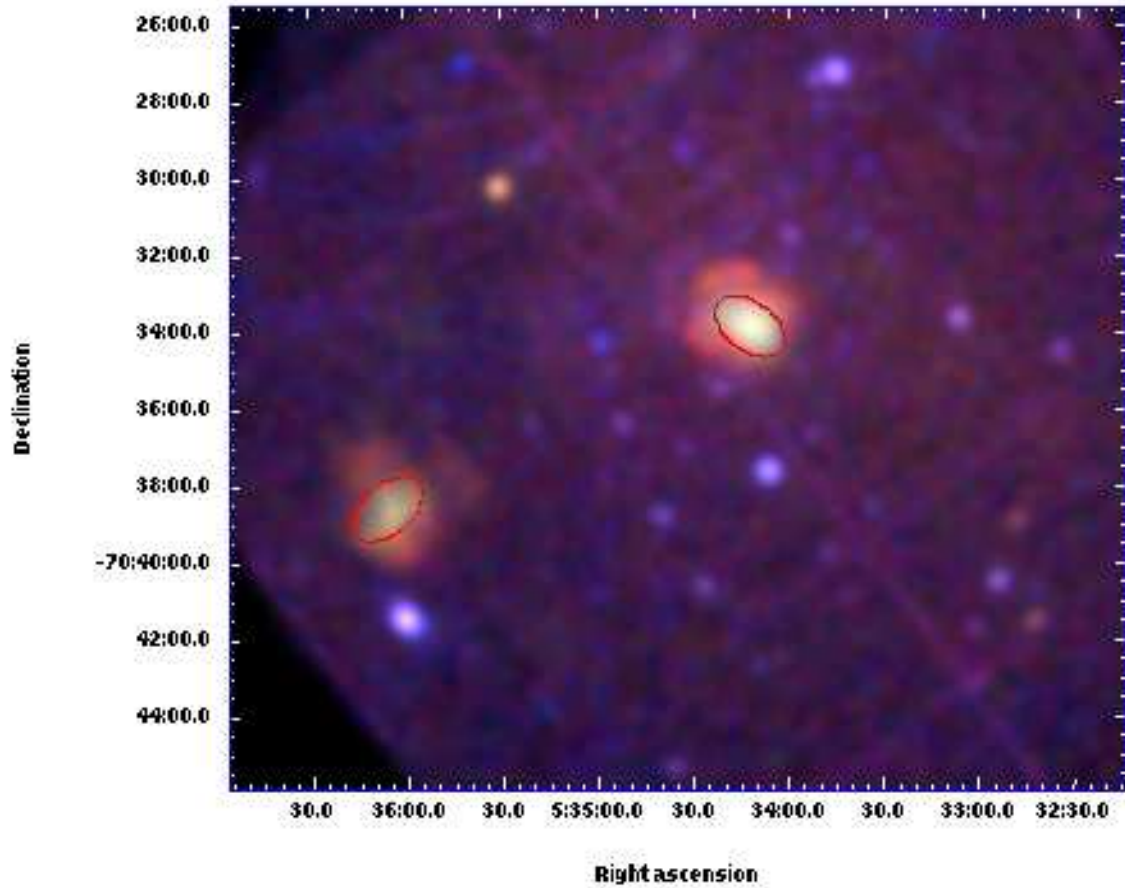


Fig. 1.— *XMM-Newton* EPIC (pn+MOS1+MOS2) image of the field of view encompassing SNRs DEM L238 (*center*) and DEM L249 (*to the east*). Data have been convolved with a $23''.5$ FWHM Gaussian. Soft (0.3–0.7 keV), medium (0.7–1.2 keV), and hard (1.2–7 keV) photons are coded by red, green, and blue, respectively. Pronounced spectral differences between prominent central emission and outer shells are apparent for both SNRs. Ellipses indicate central spectral extraction regions.

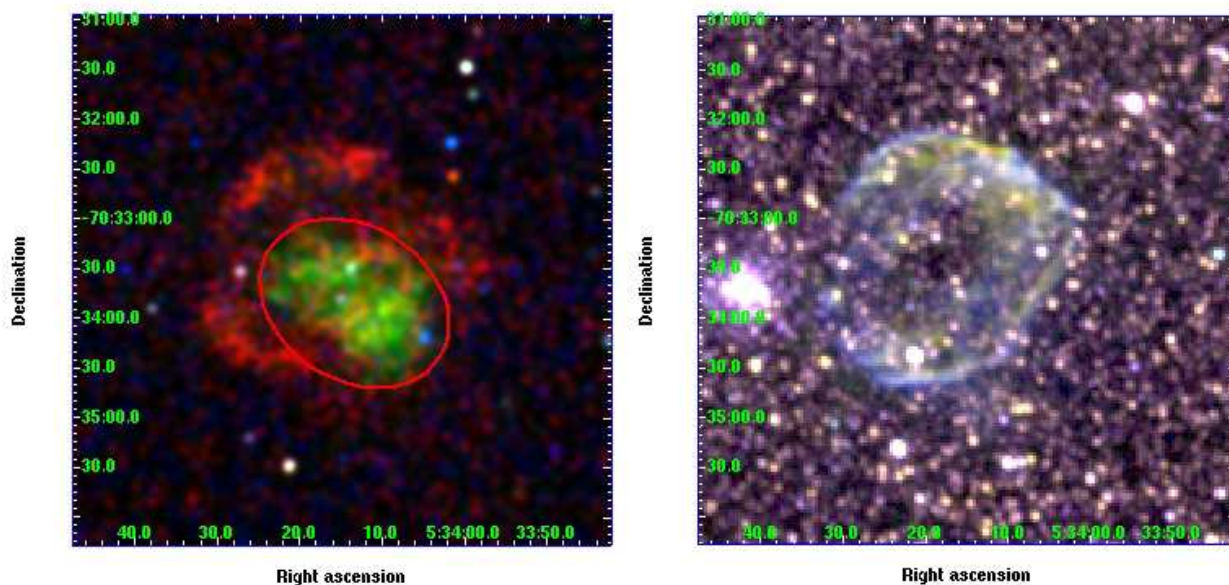


Fig. 2.— DEM L238 in X-rays (*Chandra*, left) and optical (MCELS, right). *Chandra* data have been convolved with a $5''.8$ FWHM Gaussian. Soft (0.3–0.7 keV), medium (0.7–3 keV), and hard (3–7 keV) X-ray photons are coded by red, green, and blue, respectively. MCELS [S II] $\lambda\lambda 6716, 6731$, $H\alpha$, and [O III] $\lambda 5007$ images are shown in red, green, and blue, respectively. The central spectral extraction region is shown in the *Chandra* X-ray image.

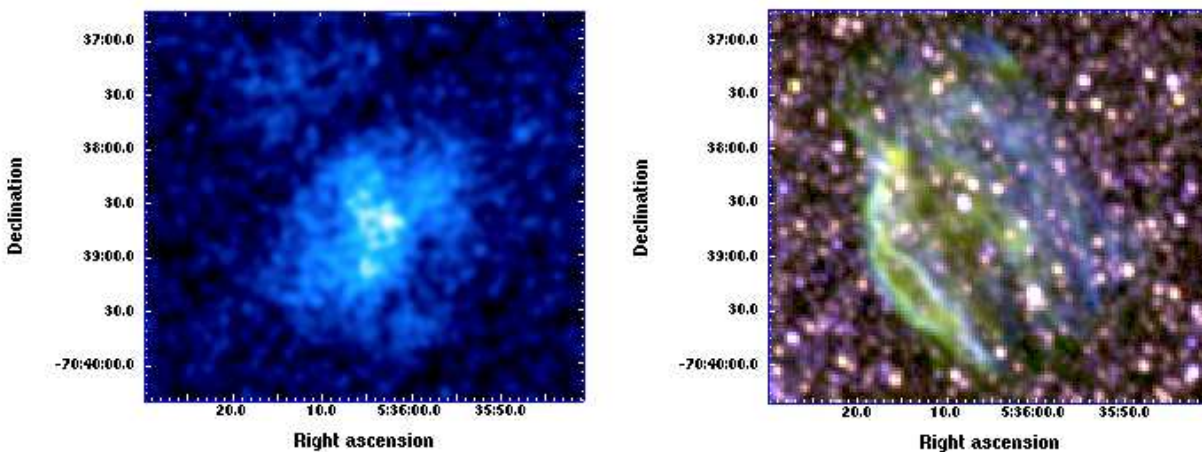


Fig. 3.— DEM L249 in X-rays (*Chandra*, left) and optical (MCELS, right). The 0.3–5 keV *Chandra* image has been convolved with a $5''.8$ FWHM Gaussian. MCELS [S II] $\lambda\lambda 6716, 6731$, $H\alpha$, and [O III] $\lambda 5007$ images are shown in red, green, and blue, respectively.

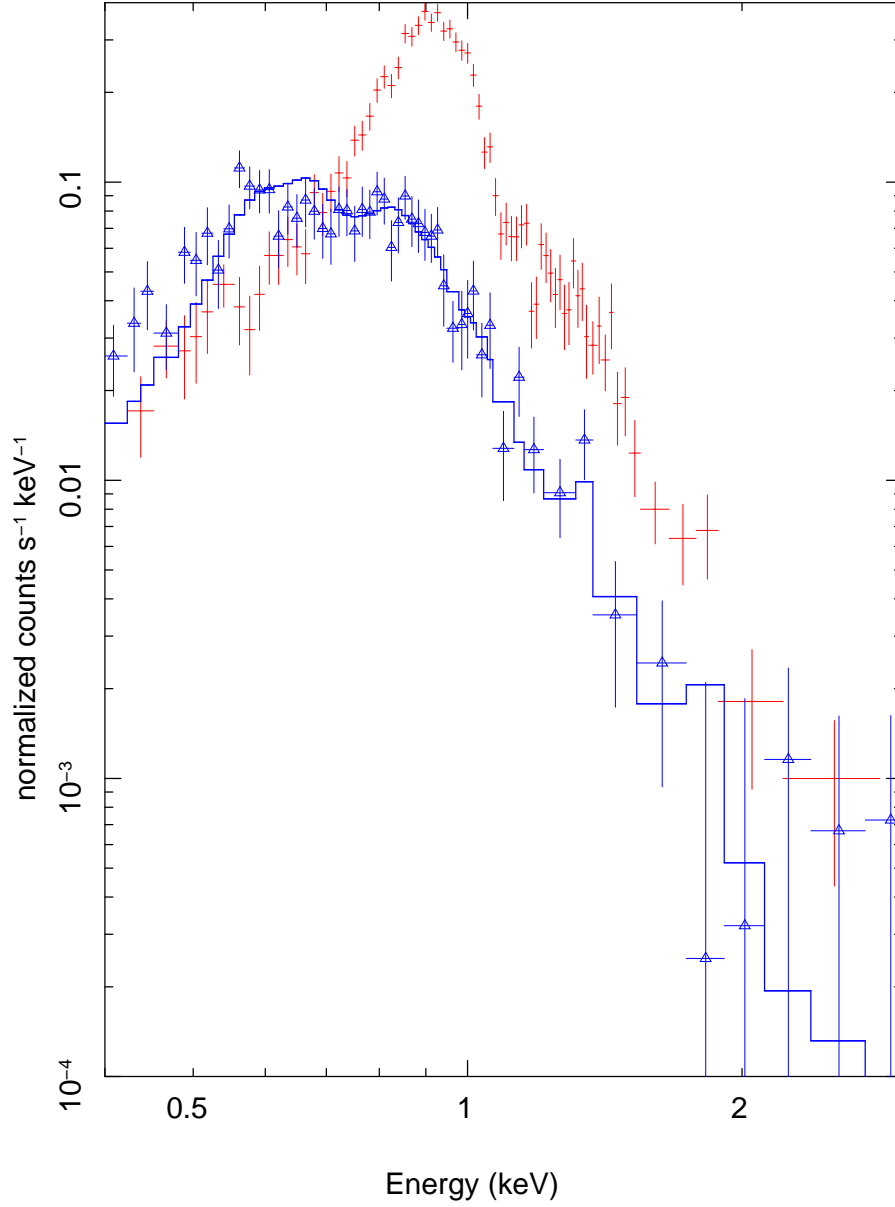


Fig. 4.— Comparison of the central (*plus signs*) and shell (*triangles*) *Chandra* spectra of DEM L238. Prominent Fe L-shell emission dominates the central spectrum. The shell spectrum is fit with a Sedov model.

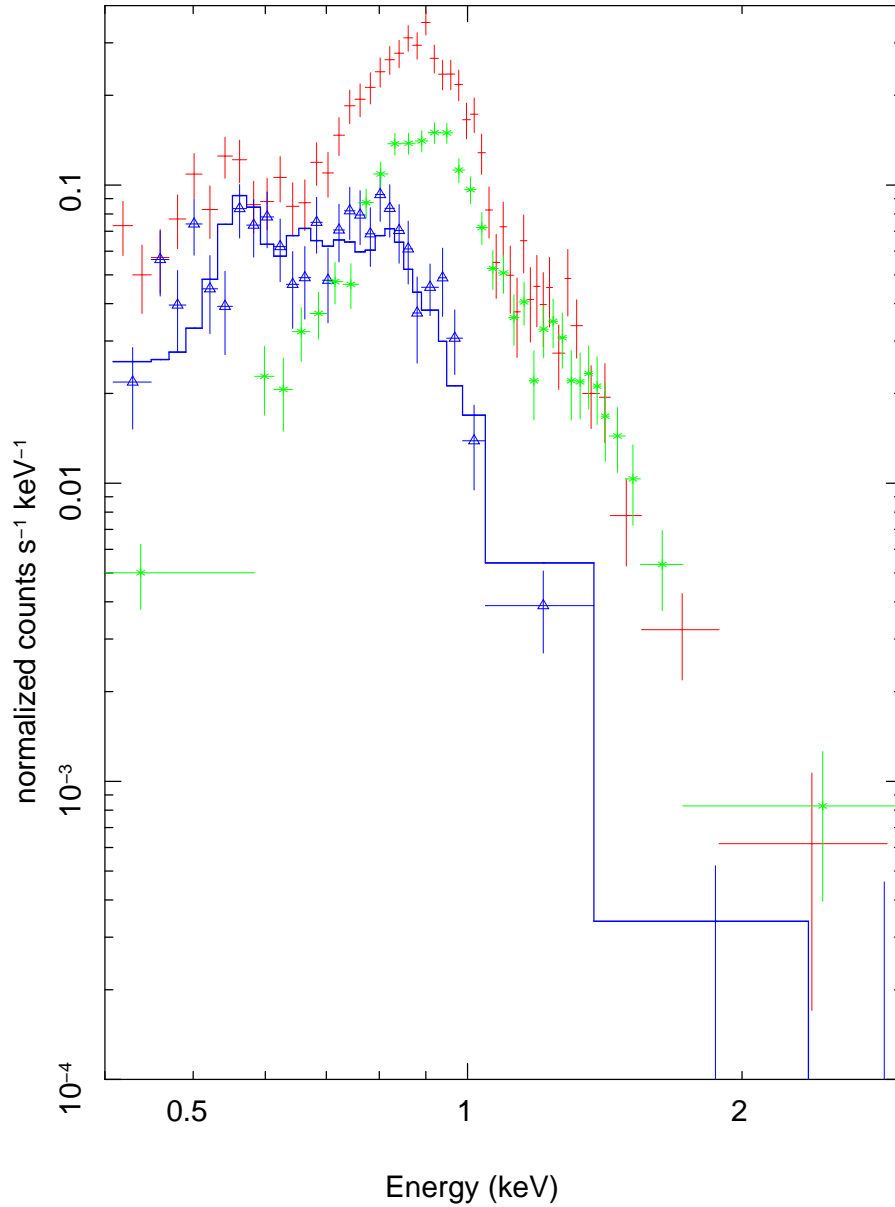


Fig. 5.— Comparison of the central (*plus signs*) and shell (*triangles*) *XMM-Newton* EPIC pn spectra of DEM L249. A prominent Fe L-shell emission dominates the central spectrum. The shell spectrum is fit with a Sedov model. The spatially integrated *Chandra* spectrum (*stars*) is also shown.

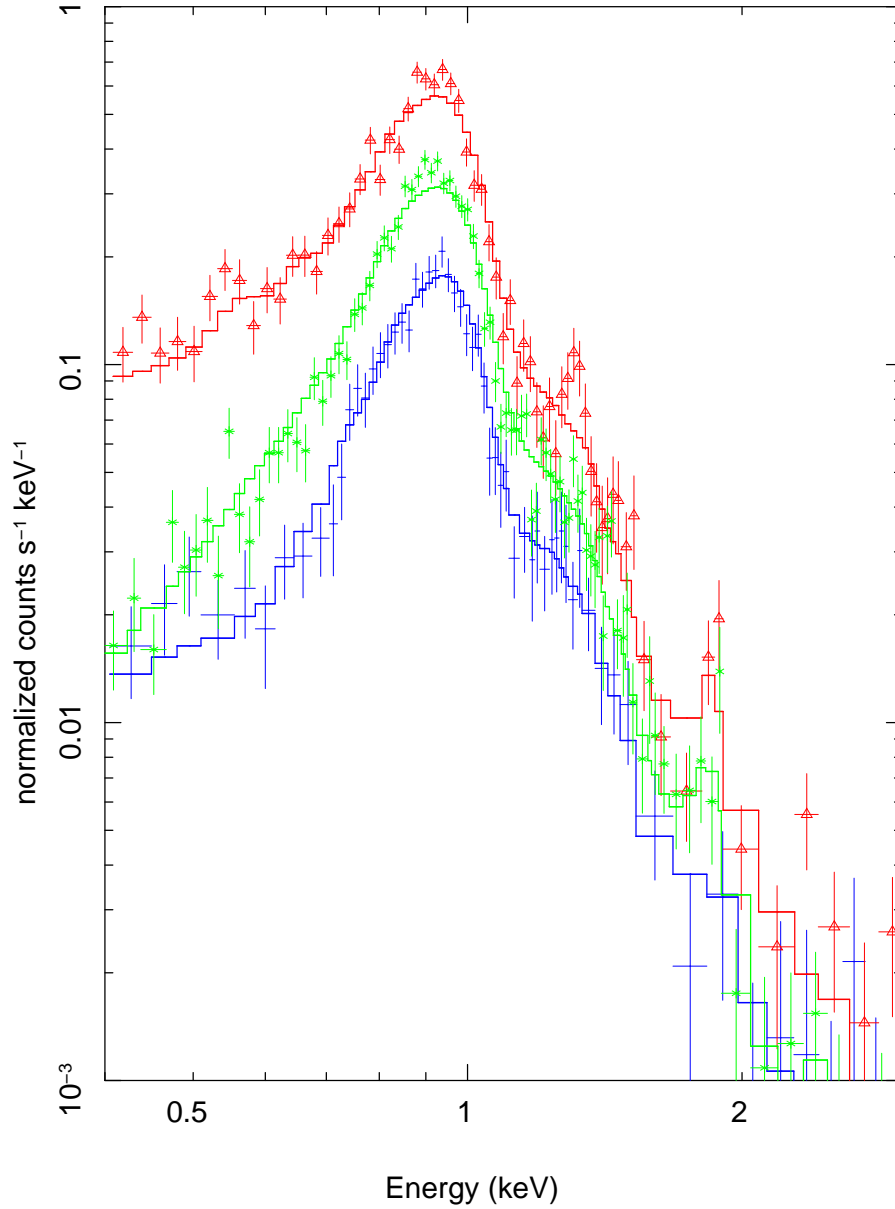


Fig. 6.— Central spectra of DEM L238 (*XMM-Newton* pn spectrum, *top*; combined MOS spectra, *bottom*; *Chandra* spectrum, *middle*). All three model fits require Fe abundance in excess of solar with respect to other elements.

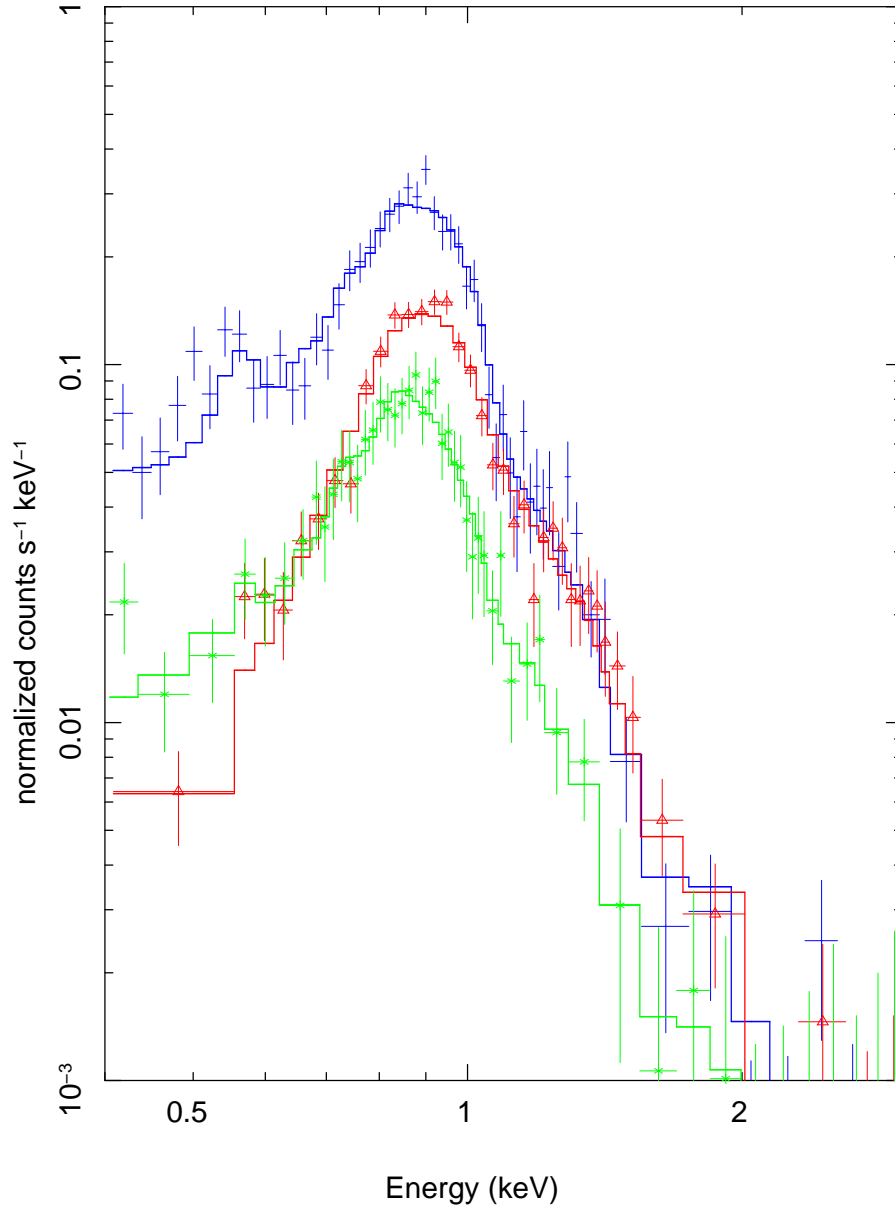


Fig. 7.— Central spectra of DEM L249 (*XMM-Newton* pn and combined MOS spectra, *top* and *bottom*; *Chandra* spectrum, *middle*: triangles). All three model fits require an Fe abundance in excess of solar with respect to other elements.

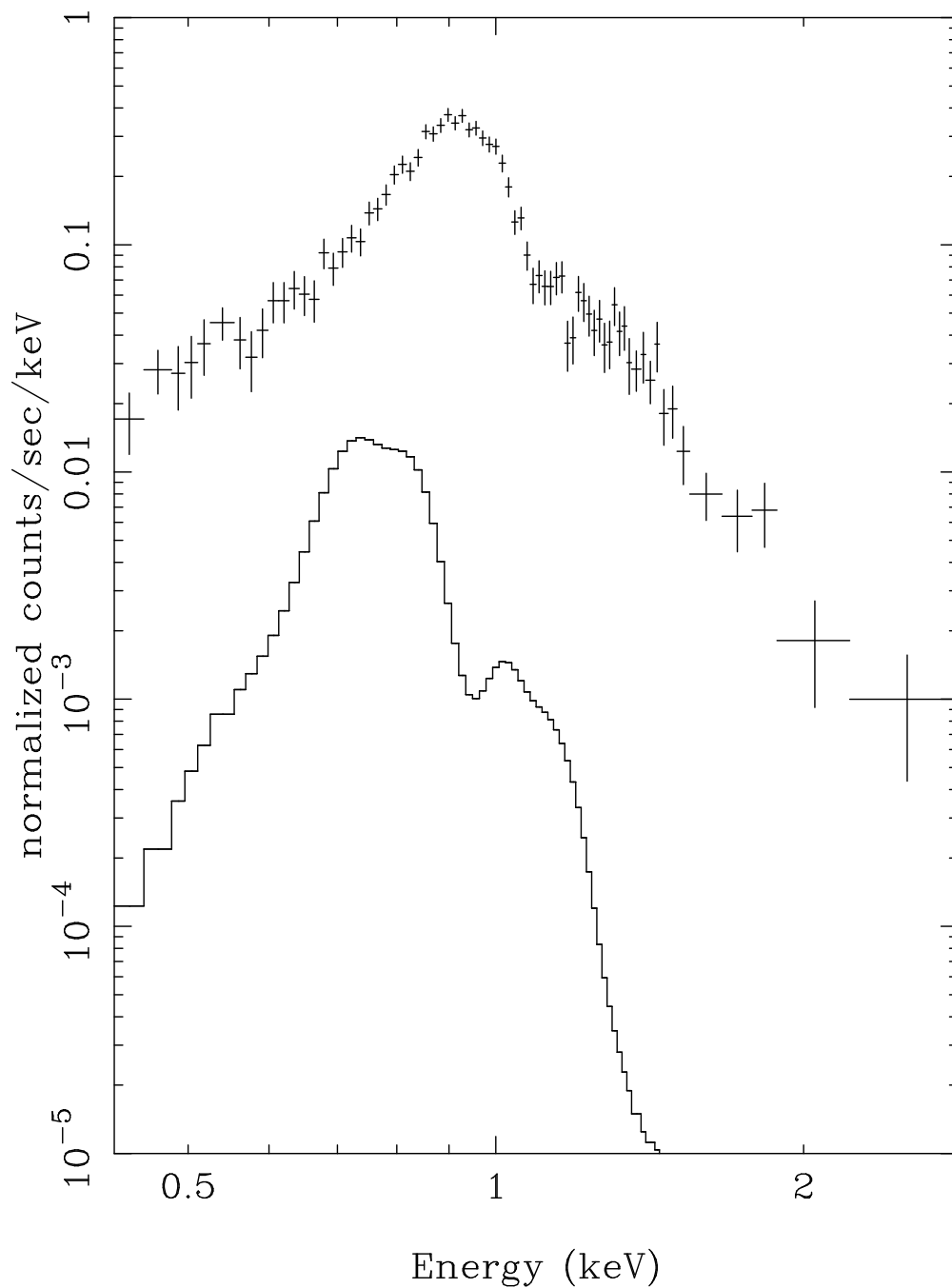


Fig. 8.— Central *Chandra* spectrum of DEM L238 (*plus signs*) compared with a model spectrum of ejecta (*solid line*) based on the simple Type Ia SNR model discussed in the text. The ejecta consist of $1.4 M_{\odot}$ of pure Fe. A dramatic discrepancy with model predictions is apparent.

Table 1. Fits to the Central Region of DEM L238

Parameters	vpshock			Sedov + vapec		
	ACIS	pn	MOS	ACIS	pn	MOS
χ^2/DOF	73/83	148/112	72/70	87/83	156/112	77/70
$(EM_S/4\pi d^2)/10^{10} \text{ cm}^{-5}$	-	-	-	$0.45^{+0.12}_{-0.12}$	$0.44^{+0.09}_{-0.09}$	$0.15^{+0.14}_{-0.12}$
kT_e keV	$0.80^{+0.03}_{-0.02}$	$0.82^{+0.04}_{-0.02}$	$0.80^{+0.03}_{-0.02}$	$0.81^{+0.01}_{-0.01}$	$0.82^{+0.01}_{-0.01}$	$0.82^{+0.02}_{-0.02}$
Fe (Ni)	$1.25^{+0.31}_{-0.24}$	$1.15^{+0.27}_{-0.19}$	$1.28^{+0.40}_{-0.26}$	$1.51^{+0.55}_{-0.33}$	$1.29^{+0.36}_{-0.24}$	$1.39^{+0.43}_{-0.28}$
$\tau/10^{12} \text{ cm}^{-3}\text{s}$	$1.17^{+0.74}_{-0.42}$	$0.83^{+0.38}_{-0.26}$	$2.3^{+7.1}_{-1.2}$	-	-	-
$(EM_C/4\pi d^2)/10^{10} \text{ cm}^{-5}$	1.81	1.38	1.40	$1.52^{+0.40}_{-0.39}$	$1.24^{+0.26}_{-0.26}$	$1.31^{+0.30}_{-0.30}$

Table 2. Fits to the Central Region of DEM L249

Parameters	vpshock			Sedov + vapec		
	ACIS	pn	MOS	ACIS	pn	MOS
χ^2/DOF	52/79	71/65	32/42	54/79	63/65	32/42
$(EM_S/4\pi d^2)/10^{10} \text{ cm}^{-5}$	-	-	-	$0.59^{+0.21}_{-0.21}$	$0.32^{+0.06}_{-0.06}$	$0.34^{+0.10}_{-0.10}$
kT_e keV	$0.75^{+0.18}_{-0.06}$	$1.25^{+0.17}_{-0.50}$	$0.71^{+0.25}_{-0.05}$	$0.73^{+0.04}_{-0.04}$	$0.77^{+0.02}_{-0.02}$	$0.69^{+0.03}_{-0.02}$
Fe (Ni)	$1.27^{+0.71}_{-0.37}$	$3.5^{+0.8}_{-2.3}$	$1.37^{+1.50}_{-0.44}$	$1.17^{+0.78}_{-0.36}$	$1.79^{+1.28}_{-0.55}$	$1.17^{+0.95}_{-0.39}$
$\tau/10^{11} \text{ cm}^{-3}\text{s}$	$3.7^{+4.5}_{-2.2}$	$0.88^{+5.30}_{-0.20}$	$4.2^{+4.1}_{-3.1}$	-	-	-
$(EM_C/4\pi d^2)/10^{10} \text{ cm}^{-5}$	1.62	0.34	1.03	$1.59^{+0.67}_{-0.63}$	$0.82^{+0.34}_{-0.34}$	$1.06^{+0.42}_{-0.46}$